

# Enhanced Fermi surface nesting in superconducting $\text{BaFe}_2(\text{As}_{1-x}\text{P}_x)_2$ revealed by de Haas-van Alphen effect

J.G. Analytis,<sup>1,2</sup> J.-H. Chu,<sup>1,2</sup> R.D. McDonald,<sup>3</sup> S. C. Riggs,<sup>4</sup> and I.R. Fisher<sup>1,2</sup>

<sup>1</sup>*Stanford Institute for Materials and Energy Sciences,*

*SLAC National Accelerator Laboratory, 2575 Sand Hill Road, Menlo Park, CA 94025, USA*

<sup>2</sup>*Geballe Laboratory for Advanced Materials and Department of Applied Physics, Stanford University, USA*

<sup>3</sup>*Los Alamos National Laboratory, Los Alamos, NM 87545, USA*

<sup>4</sup>*National High Magnetic Field Lab, Tallahassee, FL 87545, USA*

The three-dimensional Fermi surface morphology of superconducting  $\text{BaFe}_2(\text{As}_{0.37}\text{P}_{0.63})_2$  with  $T_c = 9\text{K}$ , is determined using the de Haas-van Alphen effect (dHvA). The inner electron pocket has a similar area and  $k_z$  interplane warping to the observed hole pocket, revealing that the Fermi surfaces are geometrically well nested in the  $(\pi, \pi)$  direction. These results are in stark contrast to the Fermiology of the non-superconducting phosphides ( $x = 1$ ), and therefore suggests an important role for nesting in pnictide superconductivity.

A ubiquitous ingredient in theories of high-temperature superconductivity is the role of Fermi surface (FS) nesting - a property originating from the shape of the FS which enhances quasiparticle scattering along particular directions in momentum space. FSs that support nesting are typically low dimensional with a weakly varying morphology in at least one direction in momentum space. In the case of the pnictides, it is nesting in the  $(\pi, \pi)$  direction between electron and hole FSs which is most often invoked [1–5]. From the earliest band structure calculations on the ‘1111’ compounds e.g.  $\text{LaFeAsO}$ , it was clear that this was a possible mechanism to explain both the magnetism and the superconductivity[5]. However, the ‘122’ pnictides e.g.  $\text{BaFe}_2\text{As}_2$  do not have such a strongly nested FS, yet order equally strongly in the absence of doping[3]. Furthermore  $\text{LaFePO}$ , has a FS which is measured to have well matched electron and hole pockets, and is therefore close to satisfying a nesting condition, yet has no known magnetic ordering[6, 7]. This has led several authors to invoke the local magnetic environment, particularly of the As-Fe-As tetrahedron as a route to understanding these cases [2, 3, 8]. The role of nesting, is therefore highly debated. In order to determine whether a given FS supports nesting, an intimate knowledge of the full three-dimensional morphology is required and this is the purpose of the present study.

We investigate single crystals of superconducting  $\text{BaFe}_2(\text{As}_{0.37}\text{P}_{0.63})_2$ ,  $T_c = 9\text{K}$ . The compounds  $\text{BaFe}_2\text{As}_2$  and  $\text{BaFe}_2\text{P}_2$  are isoelectronic. The former orders antiferromagnetically at  $\sim 138\text{K}$ , whereas the latter is an ordinary metal down to the lowest temperatures measured. For intermediate compositions there is a superconducting dome that peaks at  $x \sim 0.3$ , with  $T_c = 30\text{K}$ . These materials are particularly useful for dHvA studies because the disorder is weak and long mean free paths can be maintained. As a consequence, quantum oscillatory phenomena can be measured, as done recently by Shishido *et al.* [9]. This study made two im-

portant observations: first, the size of the Fermi surface increases with  $x$  beyond optimal As/P substitution and second, the effective mass decreases. However, due to the resolution limits of the data the details of the three-dimensional curvature of the Fermi surface could not be determined for the superconducting compounds and no hole pockets were observed. In the present paper we resolve the morphology of the electron pockets and that of one hole pocket. We conclude that a large amount of the FS is geometrically nested. The details revealed in this study provide compelling evidence for the role of nesting as a mechanism for high temperature superconductivity in this family of compounds.

High quality single crystals of  $\text{BaFe}_2(\text{As}_{1-x}\text{P}_x)_2$  with residual in-plane resistivity ratios  $\rho(300\text{K})/\rho(1.8\text{K}) \sim 20$ , were grown from an FeAs flux. The composition  $x = 0.63$  was determined by microprobe analysis. Torque magnetometry was performed using piezoresistive microcantilevers in fields of up to 35T in DC Bitter magnets at the NHMFL, Florida. The oscillatory part of the torque signal  $\mathbf{T} \propto \mathbf{M} \times \mathbf{B}$  originates from the dHvA effect. Each dHvA frequency is related to an extremal cross sectional area  $A_k$  of the FS in momentum space via the Onsager relation  $F = (\hbar/2\pi e)A_k$ . For simply warped, quasi-two dimensional cylinders two frequencies are expected, a maximum (‘belly’ orbit) and a minimum (‘neck’ orbit). As the angle of the field with respect to the sample is changed, these extremal orbits traverse larger sections of the Fermi surface and at particular angles, known as Yamaji angles, all cross-sectional orbits match, leading to an enhanced amplitude in the oscillation[10]. Band structure calculations were performed for the end members  $\text{BaFe}_2\text{As}_2$  and  $\text{BaFe}_2\text{P}_2$  using an augmented plane wave plus local orbital method as implemented in the WIEN2K code [11]. The composition  $x = 0.63$  does not have a structural transition at low temperature and therefore the (room temperature) experimentally determined tetragonal unit cell parameters are used. These are  $a = 3.96(3.84)\text{Å}$ ,  $c = 13.039(12.44)\text{Å}$  and  $z_P = 0.3538(0.3456)$  for the

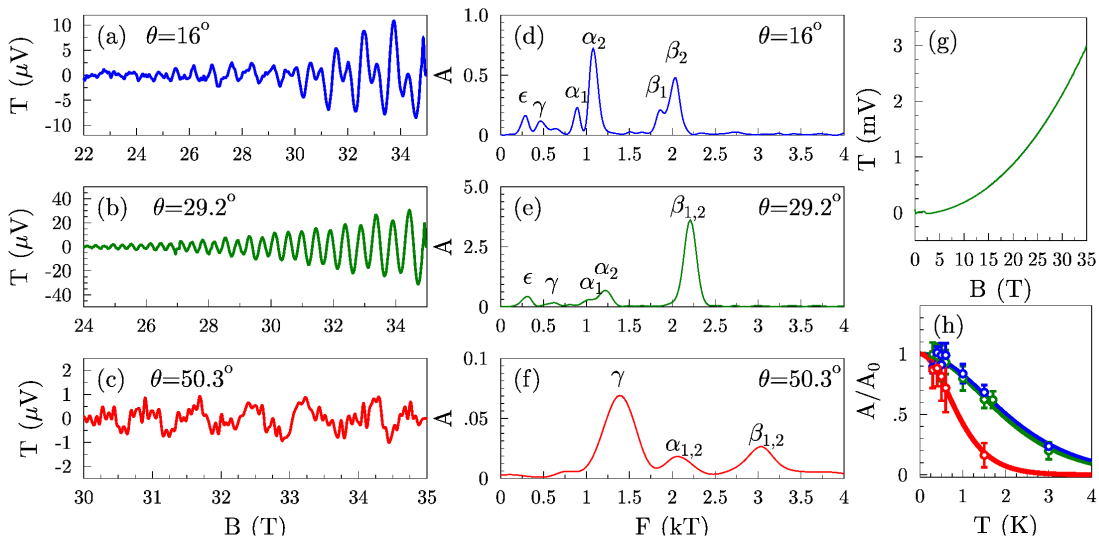


FIG. 1: The background subtracted raw data (a-c) for three different angles taken at  $T = 0.3\text{K}$ , and corresponding Fourier spectra in (d-f). The Fourier amplitudes of (e) and (f) are normalized with respect to (d) for clarity. The  $\gamma$  pockets have an enhance amplitude near  $\theta \approx 51^\circ$  probably due to a Yamaji effect. (g) gives an example of raw torque data and (h) gives the Fourier amplitude as a function of temperature with LK fits for the  $\beta$  (blue),  $\alpha$  (green) and  $\gamma$  (red) pockets, from which we determine the effective mass. (g) and (h) are taken at  $\theta = 16^\circ$ .

As(P) variants.

Fig. 1(g) shows the the raw torque signal for a single field sweep up to 35 T. dHvA oscillations are observed for fields above  $\sim 20$  T. In Fig. 1 (a-c) we show the background subtracted data at three typical angles. The Fourier spectrum is generated by implementing discrete Fourier transform methods on the signal (in inverse field) for each angle and is shown in adjacent panels. At most angles the spectrum is dominated by two (split) peaks which we label  $\alpha_{1,2}$  and  $\beta_{1,2}$ . In total five frequencies are observed, which we denote as  $\alpha_1, \alpha_2, \beta_1, \beta_2$  and  $\gamma$ . We observe a further low frequency labeled  $\epsilon$  which has some scatter about a value of 250T at most angles. However, its value is sensitive to the background subtraction and the field window used and so it is likely a noise artifact of the Fourier transform.

The calculated FS for  $\text{BaFe}_2\text{P}_2$  and  $\text{BaFe}_2\text{As}_2$  (in the tetragonal structure) is shown in Figure 2 (d) and (e) respectively. Both consist of two similarly warped concentric electron cylinders at the  $M$  point.  $\text{BaFe}_2\text{As}_2$  consists of three hole sheets while  $\text{BaFe}_2\text{P}_2$  consists of only two hole pockets centered at the  $\Gamma$  point. The hole sheets of  $\text{BaFe}_2\text{P}_2$  are much more warped than  $\text{BaFe}_2\text{As}_2$ , consistent with dHvA measurements on  $\text{SrFe}_2\text{P}_2$ [12], suggesting the latter is closer to satisfying a nesting condition. The dHvA angle dependence associated with these FSs is shown in the Figure 2(a) and (c) for  $\text{BaFe}_2\text{P}_2$  and  $\text{BaFe}_2\text{As}_2$  respectively.

Figure 2 (b) shows the angle dependence of each of the observed frequencies, broadly corresponding to the calculated band structure of the undoped compounds, though

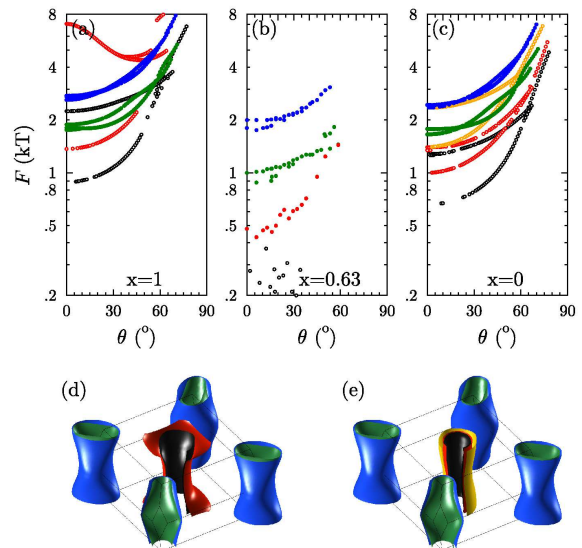


FIG. 2: (color online). (a) The dHvA angle dependence expected from LDA for  $\text{BaFe}_2\text{P}_2$ . (b) the measured angle dependence for a superconducting sample of  $\text{BaFe}_2(\text{As}_{0.37}\text{P}_{0.63})_2$ . (c) The dHvA angle dependence expected from LDA for  $\text{BaFe}_2\text{As}_2$ . The angle  $\theta = 0$  refers to field parallel to the [001] crystallographic direction, and  $\theta = 90$  to the [100] ( $\theta = 90$ ) crystallographic direction. (d) and (e) show the FS as calculated for  $\text{BaFe}_2\text{P}_2$  and  $\text{BaFe}_2\text{As}_2$ , respectively. The hole pockets are centered at the  $\Gamma$  point in the zone and the electron pockets at the  $M$  points.

substantial adjustment is required (see below). It should be noted that this discrepancy between the experimentally determined Fermi surface cross-sections and those calculated for the end members ( $x = 0$  &  $1$ ) can not be reconciled by using the experimentally determined lattice parameters for the  $x = 0.63$  compound, which only weakly affect the calculation. The strongest signal comes from the frequencies labeled  $\alpha$  and  $\beta$ . In both LaFePO [6] and SrFe<sub>2</sub>P<sub>2</sub> [12] the strongest signal was from the electrons pockets, which tend to have the longest mean free paths. It is natural to assume that this remains the case in the doped compounds and we assign these frequencies to the electron pockets.

The morphology of the pockets is best revealed by plotting the dHvA frequencies multiplied by  $\cos\theta$ , as shown in Figure 3 (a). For a two dimensional FS, the frequency dependence appears flat, whereas for warped quasi-two-dimensional cylinders the extremal cross-sections weave between the Yamaji angles. The  $\beta$  pocket appears significantly warped (a difference in neck and belly frequencies of 175T).  $\alpha$  is observable up to  $60^\circ$ , suggesting a single pocket exists around 950T. The assignment  $\alpha_1/\alpha_2$  is given to the neck/belly of this pocket and this is confirmed by the comparable effective masses (see Table I). This suggests that the pocket has a weak warping corresponding to a neck/belly difference of only 85T. The high angle data is vital for the assignment of the  $\gamma$  pocket. Approaching  $50^\circ$  the  $\alpha$  frequency abruptly turns down (see arrow in Figure 3 (a)), only to appear again near its average value a still higher angles. Simultaneously, the  $\gamma$  frequency turns upward, joining the  $\alpha$  downturn at around  $51^\circ$ . This suggests that for much of the angular range the  $\alpha$  spectrum in fact contains a third frequency, the belly of the  $\gamma$  pocket. Further confirmation of this assignment is evident in the  $51^\circ$  spectrum where the amplitude of the  $\gamma$  is enhanced beyond that of the  $\alpha$  frequency, indicating the first Yamaji angle for this pocket (see Figure 1 (f)). While it is possible that the  $\gamma$  orbit originates from the same Fermi surface as the  $\alpha$  orbit, this seems unlikely given firstly, that the  $\alpha$  orbit remains at the average value of  $\sim 950$ T at angles  $> 51^\circ$  and the effective mass of  $\gamma$  is around twice that of  $\alpha$  (see below). We conclude that  $\gamma$  is a hole pocket. Even without further analysis, it is clear that this compound has at least one hole pocket which is geometrically well matched to the inner electron pocket.

As all frequencies deviate substantially from calculations, we perform rigid band shifts on both the BaFe<sub>2</sub>As<sub>2</sub> and BaFe<sub>2</sub>P<sub>2</sub> Wien2K calculated band structure, as summarized in Figure 3 (b) and (c). The  $\beta$  pocket can be reproduced by the outer electron pocket of either band structure with relatively moderate shifts in the Fermi energy (see caption Figure 3). The average frequency of the  $\alpha$  pocket can also be reproduced by the inner electron pocket of either, but the morphology seems quite different from observations in both calculations. The

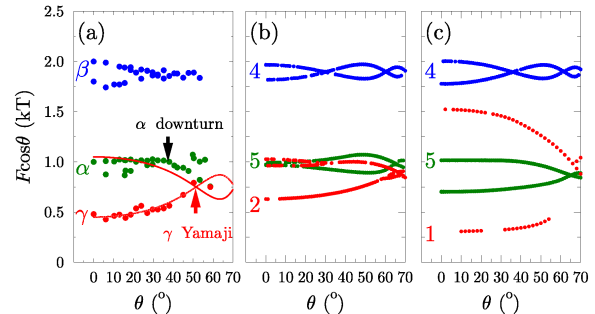


FIG. 3: (color online) (a) The observed dHvA frequencies plotted as  $F \cos \theta$ . The observed downturn in the  $\alpha$  pocket joining the Yamaji angle of the  $\gamma$  pocket is shown. (b) The best fitting rigid band shifts to the BaFe<sub>2</sub>As<sub>2</sub> band structure with Wien2K orbit numbers labeled. The  $\beta$  pocket can be broadly matched with a shift of -51meV of band 5, the  $\alpha$  pocket can be matched with a shift of -71meV of band 4 and finally, the  $\gamma$  pocket can be well approximated with a shift of +25meV to band 2, even giving a similar warping to that of the data. (c) Similar shifts to the band structure of BaFe<sub>2</sub>P<sub>2</sub> can give good approximation of the measured  $\beta$  pocket, with a -106meV shift to band 4,  $\alpha$  with a shift of -130meV to band 3. However, though a shift of +84meV to band 1 can bring the average frequency into alignment with  $\gamma$ , the pocket is significantly more warped. Larger shifts cause band 1 to form a closed 3D FS. In (a) we also show a fit of a simple cosine warped cylinder to the  $\gamma$  pocket and good agreement is achieved with the data, particularly the Yamaji angle.

band structure in BaFe<sub>2</sub>As<sub>2</sub> and BaFe<sub>2</sub>P<sub>2</sub> predicts significantly more warping than is observed, (see Figure 3 (b) and (c)). Similarly fitting the  $\gamma$  pocket, only the the BaFe<sub>2</sub>As<sub>2</sub> band structure fits the data adequately, but again the morphology is off because the Yamaji angle deviates significantly from the data (by about  $15^\circ$ ). We finally fit the  $\gamma$  frequency to simple (cosine) warped cylinder. Much better agreement is achieved with the experimental data and the Yamaji angle at  $\sim 51^\circ$  is almost perfectly matched. In summary, the experimentally determined FS can support nesting in a manner that is not obvious from band structure calculations of the end members.

The dHvA mean free path and effective mass are extracted in the conventional manner using the Lifshitz-Kosevich (LK) formula [13] and the results are summarized in Table I. As expected, the hole pocket has a significantly shorter mean free path than the electron pockets. For the effective mass, the  $\alpha$  and  $\beta$  pockets are in good agreement with those reported in Ref.9. The effective mass of  $\gamma$  has the largest error bar because of the spectral leakage from low frequency noise in the Fourier spectrum, which tends to enhance the mass. Nevertheless, it is clear that the effective mass is around twice that of the electron pockets. In order to determine the renormalization we compare our masses to that of the shifted

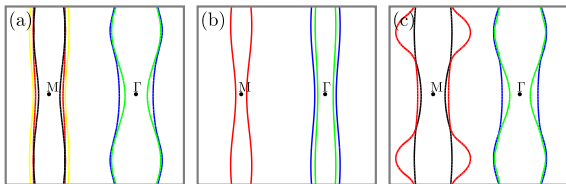


FIG. 4: (color online). Two dimensional sections through the FS in the (110) plane shown for unshifted band structures shown in (a) for BaFe<sub>2</sub>As<sub>2</sub> and (c) for BaFe<sub>2</sub>P<sub>2</sub>. In (b) we show the electron pockets after shifting the BaFe<sub>2</sub>As<sub>2</sub> bands to agree with our dHvA, and the a cosine warped cylinder is shown for the hole pocket.

band structure of BaFe<sub>2</sub>As<sub>2</sub> in Table I. We could have equally chosen to compare to BaFe<sub>2</sub>P<sub>2</sub>, in which case the renormalization would be roughly double that shown in the table. The mass enhancements are different for electron and hole pockets, being about  $\lambda = m^*/m_b - 1 \sim 0.8$  for the  $\alpha$  and  $\beta$  pockets and  $\lambda = m^*/m_b - 1 \sim 2.6$  for the  $\gamma$  orbit. These enhancements are much larger than expected from electron-phonon coupling alone ( $\lambda_{ep} \simeq 0.25$ ) [14]. Interestingly, the non-superconducting compounds have electron pockets with a greater enhancement than the holes, in contrast to the present case [12]. This study illustrates that as the superconducting dome is entered this electron/hole mass asymmetry is reversed, suggesting a vital role for many body effects.

The total electron count from  $\alpha$  and  $\beta$  is 0.1 electrons per unit cell, whereas the the  $\gamma$  pocket accounts for only .03 holes per unit cell (approximately equivalent to the  $\alpha$  electron pocket), leaving .07 uncompensated holes. As such one further hole pocket must exist that is not presently observed. Intriguingly, the contribution of the  $\alpha$  and  $\gamma$  pocket almost perfectly compensate each other, and so the remaining FS must compensate the  $\beta$  pocket. This suggests the intriguing possibility that the remaining FS is of a similar size to the  $\beta$  pocket, which may therefore sustain FS nesting between the two outer electron/hole pockets, in addition to the inner.

dHvA studies of the non-superconducting ‘122’ arsenides ( $x = 0$ ) reveal a reconstructed FS [15], whereas in the phosphides ( $x = 1$ ) they reveal an unconstructed FS but which is far from satisfying a nesting condition [12]. In stark contrast, the present work shows that the intermediate superconducting compositions have well-matched electron and hole FSs, and are therefore close to nesting. The differences between our experimental determination and the band structure calculation for each end member are summarized in Figure 4. Furthermore, the superconducting compounds have significantly smaller FSs than expected by band structure, in line with inter-band scattering theory of Ortenzi *et al.* between well-nested Fermi surfaces [16]. At smaller values of  $x$  with a higher  $T_c$  it is likely that this trend continues and

TABLE I: Measured dHvA frequencies, effective masses ( $m^*$ ) and mean free paths ( $\ell$ ), along with the values from the band structure calculations. The experimental masses were determined at  $\theta = 16^\circ$ . The band structure values are also estimated at the same angle from band structure calculations. Mean-free-paths could not be calculated separately for both neck and belly orbits due to the data resolution.

	Experiment			Calculations			
	F(kT)	$\frac{m^*}{m_e}$	$\ell$ (nm)	Orbit	F(kT)	$\frac{m_b}{m_e}$	$\frac{m^*}{m_b}$
$\gamma$	0.45	4.5(5)	12	2 <sub>min</sub>	.53	1.24	3.6
				2 <sub>max</sub>	0.86	1.72	
$\alpha_1$	.89	2.3(1)	-	5 <sub>min</sub>	1.02	1.25	1.8
$\alpha_2$	1.10	2.10(5)	48	5 <sub>max</sub>	1.04	1.31	1.6
$\beta_1$	1.80	2.1(1)	-	4 <sub>min</sub>	1.81	1.17	1.8
$\beta_2$	2.01	2.0(5)	57	4 <sub>max</sub>	1.95	1.30	1.5

the hole pockets even more closely matched the electron pockets, becoming ever more difficult to observe in dHvA studies and perhaps explaining their absence in the data of Ref.9.

In conclusion, we have measured the FS of superconducting BaFe<sub>2</sub>(As<sub>0.37</sub>P<sub>0.63</sub>)<sub>2</sub> mapping the morphology and mass enhancement in detail for both electron pockets and one hole pocket. We find that the warping of the inner electron FS is more two-dimensional than expected in the unshifted band structure, and shares a similar degree of warping to that of the hole pocket. The correlation between favorable nesting and superconductivity presently observed in BaFe<sub>2</sub>(As<sub>1-x</sub>P<sub>x</sub>)<sub>2</sub> provides strong evidence for the importance of nesting in understanding iron-pnictide superconductivity, as suggested by a number of theoretical treatments [1–5].

The authors would like to thank Antony Carrington for useful comments and E. A. Yelland for access to computer software. RMcD acknowledges support from the BES “Science in 100 T” program. Part of this work has been done with the financial support of EPSRC, Royal Society and EU 6th Framework contract RII3-CT-2004-506239. Work at Stanford was supported by the U.S. DOE, Office of Basic Energy Sciences under contract DE-AC02-76SF00515.

- 
- [1] A. V. Chubukov, D. V. Efremov, and I. Eremin, Phys. Rev. B **78**, 134512 (2008).
  - [2] K. Kuroki, H. Usui, S. Onari, R. Arita, and H. Aoki, Physical Review B **79** (2009).
  - [3] I. Mazin and J. Schmalian, Physica C (2008).
  - [4] T. A. Maier, S. Graser, D. J. Scalapino, and P. J. Hirschfeld, Physical Review B **79**, 224510 (2009).
  - [5] D. J. Singh and M. Du, Physical Review Letters **100**, 237003 (2008).
  - [6] A. I. Coldea, J. D. Fletcher, A. Carrington, J. G. Analytis, J.-H. Bangura, A F an Chu, A. S. Erickson, I. R. Fisher, N. E. Hussey, and R. D. McDonald, Phys. Rev.

- Lett. **101**, 216402 (2008).
- [7] D. H. Lu, M. Yi, S. Mo, A. S. Erickson, J. Analytis, J. Chu, D. J. Singh, Z. Hussain, T. H. Geballe, I. R. Fisher, et al., *Nature* **455**, 81 (2008).
  - [8] T. Yildirim, *Phys. Rev. Lett.* **101**, 057010 (2008).
  - [9] H. Shishido, A. F. Bangura, A. I. Coldea, S. Tonegawa, K. Hashimoto, S. Kasahara, P. M. C. Rourke, H. Ikeda, T. Terashima, R. Settai, et al., 0910.3634 (2009).
  - [10] K. Yamaji, *Journal of the Physical Society of Japan* **58**, 1520 (1989).
  - [11] P. Blaha, K. Schwarz, G. K. H. Madsen, D. Kvasnicka, and J. Luitz, *WIEN2K, An Augmented Plane Wave + Local Orbitals Program for Calculating Crystal Properties* (Karlheinz Schwarz, Techn. Universität Wien, Austria, 2001).
  - [12] J. G. Analytis, C. M. J. Andrew, A. I. Coldea, A. McCollam, J. Chu, R. D. McDonald, I. R. Fisher, and A. Carrington, *Physical Review Letters* **103**, 076401 (2009).
  - [13] D. Schoenberg, *magnetic Oscillations in Metals Cambridge University Press*, London, 1984.
  - [14] L. Boeri, O. Dolgov, and A. Golubov, *Physical Review Letters* **101** (2008).
  - [15] J. G. Analytis, R. D. McDonald, J. Chu, S. C. Riggs, A. F. Bangura, C. Kucharczyk, M. Johannes, and I. R. Fisher, arXiv: 0902.1172.
  - [16] L. Ortenzi, E. Cappelluti, L. Benfatto, and L. Pietronero, *Physical Review Letters* **103** (2009).